Isothermal and Non-Isothermal Reduction Behaviors of Iron Ore Compacts in Pure Hydrogen Atmosphere and Kinetic Analysis

Abourehab Hammam [1,2] · Ying Li [1] · Hao Nie [1] · Lei Zan [1] · Weitian Ding [1] · Yao Ge [1] · Meng Li [1] · Mamdouh Omran [1,2,3] (iD) · Yaowei Yu [1]

Abstract

This study examines the isothermal and non-isothermal reduction behaviors of iron ore compacts in a pure hydrogen atmosphere and compares the results obtained during the reduction process by CO. The different phases accompanying the reduction reactions were identified using X-ray diffraction (XRD) and its morphology was microscopically examined. In isothermal experiments, temperature plays a significant role in the reduction process. At any given temperature, the reduction rate during the initial stages is higher than that during the final stages. The reduction rate in H_2 atmosphere was faster than in CO gas. The comparison of activation energy values suggested that reduction with H_2 is more efficient than with CO. At the same temperature, the time required to achieve a certain degree of reduction was lower when using H_2 gas than CO atmosphere. In non-isothermal tests, the heating rate has a significant effect on the reduction rate and reduction extent. At the same heating rate, the degree of reduction was higher in H_2 atmosphere than in CO gas. Based on experimental data, the parameters of reaction kinetics were deduced by application of model-free and model-fitting methods. The reduction in H_2 atmosphere was controlled by nucleation model (Avrami-Erofeev model), while the CO reduction reaction was controlled by gas diffusion.

Keywords Hydrogen gas · Isothermal reduction · Non-isothermal reduction · Kinetics and mechanism

1 Introduction

Iron and steelmaking sector is one of the most important sectors due its great impact on the global growth, economy, and development. In recent years, the steel production rate has increased sharply [1]. By 2050, steel demand is expected to increase to 1.5 times higher than the current levels in order to meet the needs of a growing population [2, 3]. About 70% of the total steel production relies directly on inputs from coke and coal [3, 4]. The CO_2 emission from iron and steelmaking was 2.3 billion tons in 2007, while by 2050 it is expected to reach 3.0 billion tons [5]. Nowadays, the main challenges for the steel industry are energy consumption and environmental pollution. Therefore, the growing of the steel sector requires serious attention in order to establish processes that are economically viable and environmentally friendly [6].

Direct reduction (DR) process is one of the promising alternative ironmaking processes to effectively reduce CO_2 emissions. Therefore, recently great efforts have been paid to develop DR processes. The natural gas and non-coking coal are main reductants and sources of energy used in these DR processes [7]. In Sweden, three companies, steel manufacturer SSAB, mining company LKAB, and energy company Vattenfall, are exploring the use of hydrogen in steel production processes. This technology is known as Hydrogen Breakthrough Ironmaking Technology (HYBRIT) and aims to totally replace the coke with hydrogen gas [8, 9]. In view of increasing demand for direct reduced iron in the manufacturing of steel, a good deal of emphasis is being given to promote the study of DR process [10]. Recently, attention has been paid on studying the kinetics and mechanisms of iron oxide reduction in the different gas mixture such as H_2, CO, and CO/H_2 gas mixtures.

✉ Mamdouh Omran
mamdouh.omran@oulu.fi

✉ Yaowei Yu
Yaoweiyu@shu.edu.cn

1   State Key Laboratory of Advanced Special Steel, Shanghai Key Laboratory of Advanced Ferrometallurgy, School of Materials Science and Engineering, Shanghai University, Shanghai, China

2   Central Metallurgical Research and Development Institute (CMRDI), P.O. Box 87, -Helwan, Cairo, Egypt

3   Process Metallurgy Research Group, Faculty of Technology, University of Oulu, Oulu, Finland

The effect of H_2-H_2O on the iron ore pellet reduction was isothermally investigated at 700–1100 °C [11]. The influence of a mixture of CO-CO_2-H_2-H_2O-N_2 reducing gas was compared with that of a mixture of reducing gas containing only CO-CO_2-N_2. The results indicate that the reduction degree increases with increasing the temperature in both reducing gas atmospheres. Spreitzer et al. [12] indicated that, by increasing H_2 content in the reducing atmosphere, the reduction degree of pellets improved, owing to improving the diffusion rate due to hydrogen's small molecular size.

El-Geassy et al. studied the reduction mechanism of iron oxide in H_2/CO mixtures in a temperature range of 800 to 1100 °C [13]. They concluded that the reduction with either CO or CO/H_2 gas mixtures is controlled by mixed mechanism (combination of chemical reaction and gaseous diffusion) with a greater contribution of the gaseous diffusion as the CO content increases in the gas mixture. El-Geassy investigated the influence of doping with CaO and/or MgO on the stepwise reduction of hematite compacts [14]. They found that, during the first and second step (Fe_2O_3–Fe_3O_4 and Fe_3O_4–FeO), the reduction rate increased in its early stages when any doping oxide was used. At later stage (FeO-Fe), the presence of MgO impeded the reduction process. El-Geassy et al. [15, 16] studied the volume change of iron oxide compacts and the influence of gas composition on reduction behavior at 800 to 1100 °C. They found that increased CO content in the gas mixture had a significant influence on swelling and maximum swelling (224%) was observed for samples reduced at 900 °C. Decreasing CO content in the gas mixture led to a decreased in swelling by 24% in pure H_2 atmospheres.

The reduction of iron ore with gas takes place in either two or three stages, depending on the applied temperature. At temperature > 570 °C, hematite is first reduced to magnetite then to wustite in a non-stoichiometric phase ($Fe_{1-y}O$) and finally to metallic iron. At temperatures ≤ 570 °C, hematite is reduced to magnetite and then directly transformed into metallic iron [17]. Daniel et al. [18] study the reduction kinetics of hematite iron ore fines by hydrogen gas using a laboratory fluidized bed reactor in a temperature range 873–1073 K. They concluded that the reduction takes place in three steps: Fe_2O_3-Fe_3O_4, Fe_3O_4-FeO, and finally FeO-Fe. Lin et al. [19] were using temperature-programmed reduction (TPR) methods to study the reduction mechanism of iron oxide with hydrogen. They found that reduction takes place in two steps: the first step (Fe_2O_3-Fe_3O_4) was confirmed by the unimolecular model, while the second step (Fe_3O_4-Fe) matched a nucleation two-dimensional model according to the Avrami-Erofeev model.

Piotrowski et al. [20] investigated the effect of gas composition on the kinetics of iron oxide reduction by hydrogen. It was found that the reaction rate increases with both temperature and the hydrogen content. The reduction was initially proved to be a surface-controlled process. Once a thin layer of lower oxides (magnetite and wustite) formed on the surface,

then the reduction mechanism shifts to control by gas diffusion. Bonalde et al. [21] investigated the reduction kinetics of hematite pellets at 850 °C. The reduction experiments were carried out using H_2, CO, and gas mixture. Reduction rates with H_2 were better than with CO. Skorianz [22] studied the reduction behavior of different iron ores with different porosities in a fluidized bed reactor. The reducibility of ores was demonstrated to be in this order: limonitic with the highest porosity hematite then magnetite with low porosity.

During the industrial DR process, the reduction of iron ore happens at variable temperatures (non-isothermal) rather than at a constant temperature (isothermal). Therefore, it is vital to understand the kinetic analysis of non-isothermal conditions, which would be a better choice for non-blast furnace ironmaking, i.e., the DR process and hydrogen metallurgy. The latter in recent years becomes quite popular in the global steel industry and in academic field.

Non-isothermal reduction reaction of Fe_2O_3 nanopowder by hydrogen was studied at various heating rates [23]. It was found that the reduction process takes place in the sequence of Fe_2O_3 to Fe_3O_4 and Fe_3O_4 to Fe. The apparent activation energy Ea for kinetic analysis was determined using the Kissinger-Akahira-Sunose (KAS) method. During the reduction step (Fe_3O_4 to Fe), the reduction rate was retarded by sintering of oxide particles leading to an abrupt increase of activation energy. As the volume fraction of the metallic iron increased, the reaction rate accelerated, which can be attributed to the catalytic role of the reduced Fe particles facilitating reduction of the adjacent oxide particles. Jie Dang et al. [24] investigate the reduction of titanomagnetite (TTM) powders by hydrogen gas under a non-isothermal condition by using thermogravimetry (TG). It was found that the reduction of TTM proceeded via a dual-reaction mechanism. The first one was the reduction of TTM to wustite and ilmenite, while the second reaction was the reduction of wustite and ilmenite to metallic iron and titanium dioxide. The calculated apparent activation energies were 90–98 and 115–132 kJ/mol for the first and second reactions, respectively.

Tiernan et al. [25] investigate the reduction kinetics of iron oxide catalysts under non-isothermal conditions. Both temperature-programmed reductions (TPR) and constant rate temperature-programmed reduction (CR-TPR) were utilized. Fe_2O_3 was found to reduce to Fe in two steps: Fe_2O_3-Fe_3O_4 and Fe_3O_4-Fe. The rate-controlling mechanism was described by the random formation and growth of nuclei. CR-TPR profiles allowed the measurement of apparent activation energies as a function of the reduction extent. For the first step, Ea was found to be 96 kJ/mol. For the second step, Ea decreased from 69 to 59 kJ/mol as the reduction proceeded.

The present study aims to investigate the isothermal and non-isothermal reduction kinetics of iron ore fines in a hydrogen atmosphere, comparing the experimental results of H_2 with those of CO. The study will predict the kinetics and

correlate these predictions with the morphological structure to deduce the reduction mechanisms.

2 Experimental Technique

2.1 Materials

The iron ore fines used in this study were collected from a DR plant (Al-Ezz El-Dekheila Steel Company, Alexandria) in the form of a waste material produced by the transportation and handling of pellets. The sample was characterized using X-ray diffraction (XRD; PW 1730 with Cu radiation, $\lambda = 1.5$Å, at 40 kV and 30 mA). Figure 1 shows that hematite was the main mineral phase in the sample.

The chemical composition of the sample was identified using X-ray fluorescence (XRF advanced Axios, Netherlands); the results are listed in Table 1. Iron (III) oxide (Fe_2O_3) was the main oxide in the sample accounting for about 96 wt.%.

Size analysis was conducted for representative sample of iron ore fines to determine the size distribution. A laboratory "Wedag" Ro-tap sieve shaker was employed for dry screening of sample. Shaking was performed at 60 Hz for 20 min, after which the weight of oversize on sieves was recorded to calculate weight passed and/or retained. The particle size distribution in the iron ore fine sample is shown in Table 2, indicating that more than 60% of the sample consisted of particles in the < 100 μm size range.

The structure of the sample was examined using both a scanning electron microscope (SEM JEOL, JSM-5410, 10Kv) and reflected light microscope (RLM, Zeiss Axio Scope A1) as shown in Fig. 2a and b, respectively. The SEM image shows that the structure contains fragments of different shapes and sizes which came out of pellet disintegration and abrasion during pellet transportation and handling. The RLM photomicrograph indicates that the internal

Table 1 Chemical composition of iron ore fine sample

Elements	wt.%	Oxides	wt.%
Fe_2O_3	96.01	K_2O	0.024
SiO_2	1.62	P_2O_5	0.039
CaO	0.977	MnO	0.093
MgO	0.099	V_2O_5	0.051
Al_2O_3	0.655	Cr_2O_3	0.021
TiO_2	0.082	SrO	0.012
SO_3	0.054	NiO	0.017
Na_2O	0.011		

structure includes a relatively dense matrix with more or less homogeneously distributed pores.

2.2 Compact Preparation

In order to ensure that the compacts were of uniform size and shape, iron ore fines were compressed in a stainless steel cylindrical mold. The compacts were created by mixing iron ore fines with 6% distilled water as a binder. Then, equal weights (2 g) of the mixture were compressed at 10 atm (10 kg/cm^2) using a hydraulic press. Compacts with a diameter of 10 mm and a height of 12 mm were dried at 110 °C and kept in a dissector for subsequent analysis.

The total reducible oxygen content (w_0) of iron ore fines was estimated by preliminary reduction experiment at 1100 °C using H_2 gas until the weight of the sample reaches constant (Eq. 1). Then, the extent of the reduction at time t ($R_t\%$) was calculated using Eq. 2.

$$w_0 = w_i - w_f \tag{1}$$

$$R_t = \frac{(w_i - w_t)}{w_0} * 100 \tag{2}$$

where w_i is the weight of the sample at zero time, w_t is the

Fig. 1 X-ray diffraction of iron ore fine sample
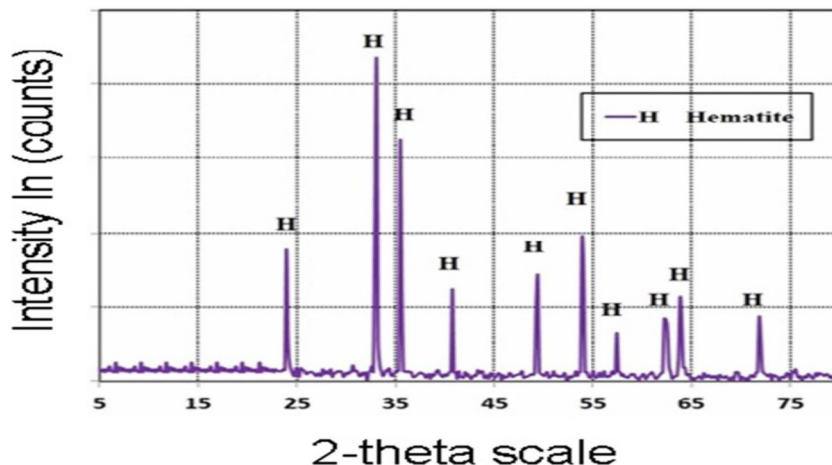
Table 2 Particle size distribution of iron ore fines (mass %)

	Size fraction/μm						Total
	(− 250 + 205)	(− 205 + 150)	(− 150 + 105)	(− 105 + 75)	(− 75 + 45)	(− 45)	
Mass%	7.47	10.48	16.74	34.52	20.54	10.25	100

weight of the sample at time t, and w_0 is the total oxygen content.

2.3 Reduction Apparatus and Procedure

2.3.1 Reduction System and Procedure

Thermogravimetry (TG) was used to measure both isothermal and non-isothermal reactions. The reduction apparatus is illustrated in Fig. 3. The main parts of the reduction system include a vertical tube furnace (F), fitting with an alumina reaction tube (A) and an automatic sensitive balance (B) at the top. The data from the balance (O) is connected to a recording unit (R) for continuous monitoring of the weight loss of samples during the experiments. The control parts (K) are two thermocouples T1 and T2. The temperatures of the furnace and sample are measured with two different thermocouples, one in the hot zone (T1) and the other behind the sample (T2). A gas supply system and gas purification unit (E) is used to remove moisture and other contaminants from the gases.

2.3.2 Isothermal Experimental Procedure

In experiments, the furnace is heated up to a target temperature and maintained at this temperature for around 5 min. Pure argon (Ar) gas is then introduced into the furnace at a flow rate of 1.0 l/min. After that, the sample is placed in a basket which hangs from the balance arm by a wire; then, the basket is positioned in the hot zone of the furnace. Under these conditions, Ar gas is replaced by 1.0 l/min of H_2. During the experiment, the weight loss of the sample due to O_2 removal

is continuously recorded until the weight remains constant. At the end of the experiment, H_2 gas is replaced by Ar gas and the furnace is cooled back down to room temperature. The reduced sample is taken out and kept in a desiccator for later characterization.

2.3.3 Non-Isothermal Experimental Procedure

In these tests, the furnace is first flushed with Ar at a flow rate of 0.2 l/min and held in this condition for 5 min. Then, the Ar gas switched to H_2, which introduced at a flow rate of 1.0 l/min. The sample is heated in the reducing gas from room temperature to 1000 °C at different heating rates (5, 10, 15, and 20 °C/min). At the end of the experiment, the H_2 is replaced by Ar gas and the furnace is cooled back down to room temperature. The reduced sample is taken out and kept in a desiccator for later characterization.

3 Results and Discussion

3.1 Isothermal Reduction

3.1.1 Reduction Behavior

The reduction curves of Fe_2O_3 compacts by H_2 gas at temperatures 800 to 1100 °C are illustrated in Fig. 4. For any given reduction temperature, the rate of reduction is highest in the early stages and gradually decreases until the end of the reduction reaction. At low temperatures, the reduction takes longer and the reduction time decreases as reduction

Fig. 2 Photomicrographs of iron ore sample. **a** SEM (× 5000). **b** RLM (× 100)
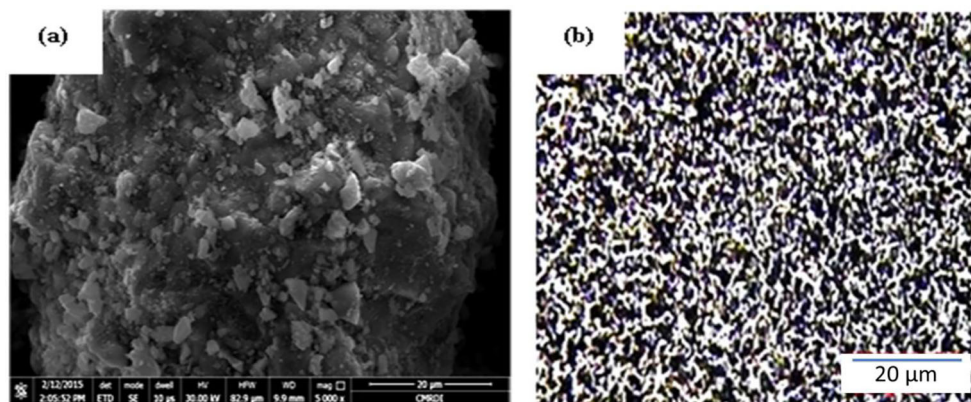
Fig. 3 Schematic diagram for reduction apparatus of TGA system
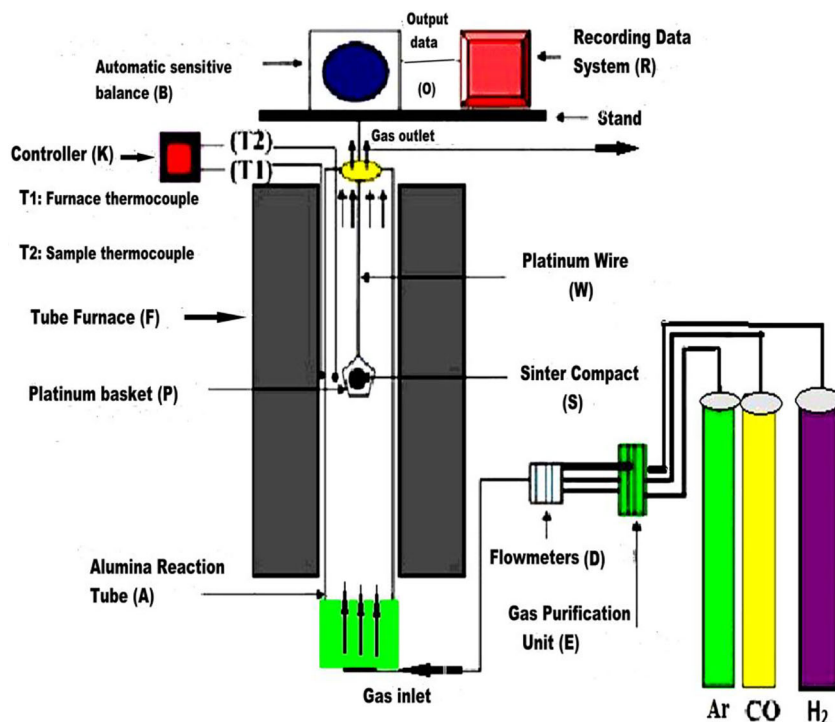
temperature increases. Furthermore, the extent of reduction at the maximum values (the plateau) appears to increase with rise in temperatures. The high degree of reduction during the initial and intermediate stages can be attributed to the reduction of Fe_2O_3 to Fe_3O_4 and from Fe_3O_4 to Fe. The relatively slowing down of the reduction rate during the final stages is caused by the reduction of FeO to Fe.

In the case of reduction using CO at temperatures 80–900 °C, samples did not complete reduction and stopped at different extents of reduction, depending on the applied temperature [26]. Moreover, during experiments, an increase in the weight of the compacts was observed. This phenomenon previously observed elsewhere [27] indicates that the rate of carbon participation as a result of the thermal decomposition of carbon

monoxide ($2CO = C + CO_2$) is greater than the rate of oxygen removal.

The microstructure of the completely reduced compacts with H_2 at 950 and 1100 °C is given in Fig. 5a and b, respectively. Figure 5a illustrates that the structure includes elongated grains of metallic iron and coalesces to each other with separated small macropores. As the reduction temperature increases, the matrix structure became relatively dense due to the coalescence and connection of metallic grains as shown in Fig. 5b.

3.1.2 Kinetics and Mechanism of Iron Ore Reduction

According to previous literature [12], iron ore reduction is supposed to take place from the surface and progress to the

Fig. 4 Reduction behaviors of iron ore compacts at 800–1100 °C by pure H_2
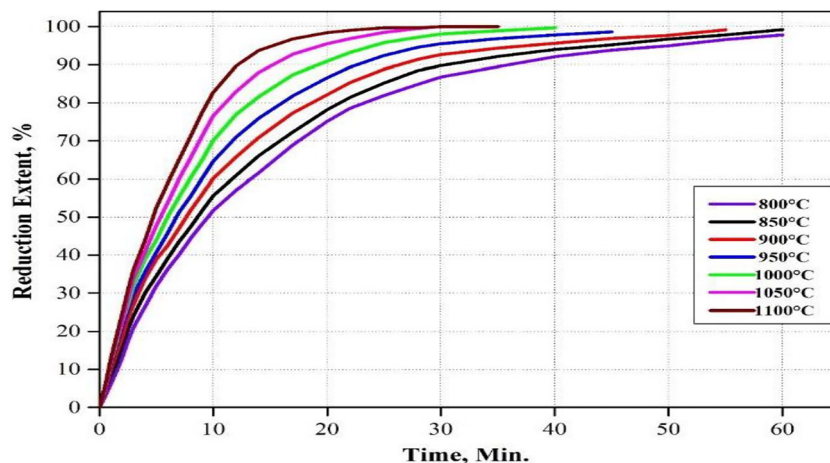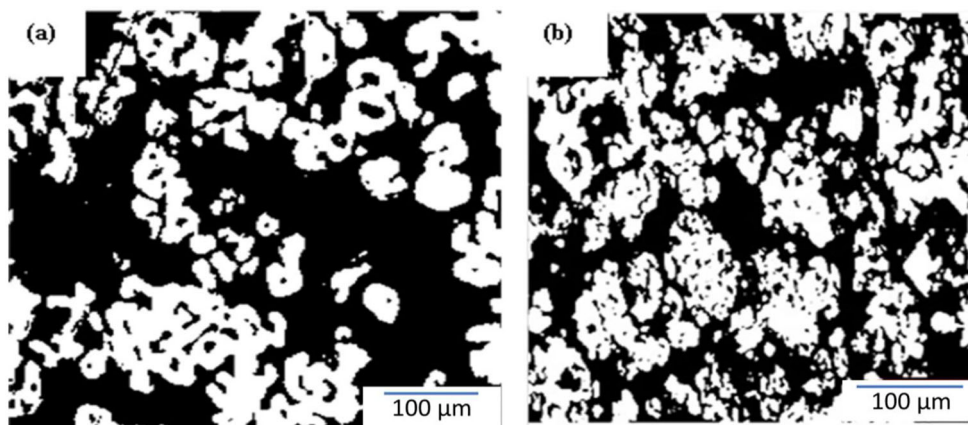
core and the diameter of the unreacted core becomes smaller
and smaller until zero. The reduction mechanisms of iron ore
during both the initial and final stages can be deduced from the
correlations between the apparent activation energy values,
the gas-solid chemical reaction, and the microstructure of the
reduced samples in the reduction procedure [26, 28–31]. The
kinetics of iron ore reduction can be described using a shrink-
ing unreacted core model to elucidate the reduction reaction.
In the beginning, iron ore particles are assumed to have 100%
hematite and have an initial diameter. With the increase in the
reduction reaction, a product layer of iron is created and the
unreacted core of pellet particle is decreased to a smaller di-
ameter. A layer of reactant gas exists at the initial diameter of
the iron ore particle. A chemical reduction reaction can be
divided into three stages: external diffusion, internal diffusion,
and chemical reaction. The chemical reaction is expressed by
the Arrhenius equation in Eq. 3:

$$K_r = K_o \, e^{-Ea/RT} \tag{3}$$

where K_r is the reaction rate constant, K_o is the frequency
factor, Ea is the apparent activation energy, R is the gas con-
stant, and T is the absolute temperature.

The rate of reaction (K) is calculated using the isothermal
curves given in Fig. 4. The relationships between ln$K$ and
(1/T) are plotted during both the initial stages (5–15%) and
the final stages of reduction (85–95%) as shown in Fig. 6. The
computed apparent activation energy values for the reduction

by H$_2$ and CO are listed in Table 3. The comparison of acti-
vation energy values indicated that reduction with H$_2$ is more
efficient than with CO.

At the initial stages, the Ea value indicates that the reduc-
tion process seems to be controlled by a mixed mechanism of
gaseous diffusion and interfacial chemical reaction. During
the final stages, the Ea value reveals that the reaction is con-
trolled by interfacial chemical reaction and this matched with
other studies [17, 26, 32].

The mathematical models that are typically adopted for
predicting kinetics mechanisms in heterogeneous gas-solid
reactions and the grain model developed by Szekely et al.
[28] are the most accurate one for the similar experimental
conditions, in which long cylinder samples are produced from
compacting fines of solid materials. Gaseous diffusion, inter-
facial chemical reaction, and mixed control mathematical for-
mulae have been tested in this study to evaluate the control
stage in the overall reduction process. The three mathematical
kinetic equations are as follows [28, 32]:

(a) For gaseous diffusion mechanism:

$$K = X + (1-X) \ln (1-X) \tag{4}$$

(b) For chemical reaction mechanism:

$$K = 1-(1-X)^{0.5} \tag{5}$$

(c) For mixed control mechanism:

$$K = 1-(1-X)^{0.5} + X + (1-X)\ln(1-X) \tag{6}$$

where K and X express the rate of reaction and the fractional
reduction degree, respectively.

In order to confirm the reduction mechanism prediction
from the activation energy values, the above chemical reaction

Table 3 Apparent Ea values calculated at the initial and final stages of
reduction

Reducer of Fe$_2$O$_3$ compacts	Ea values (kJ/mole)	
	At 5–10% extents	At 85–95% extents
H$_2$	28.34	41.15
CO	39.23	54.19 [26]

Fig. 6 Arrhenius plots for Fe_2O_3 compacts reduced by H_2
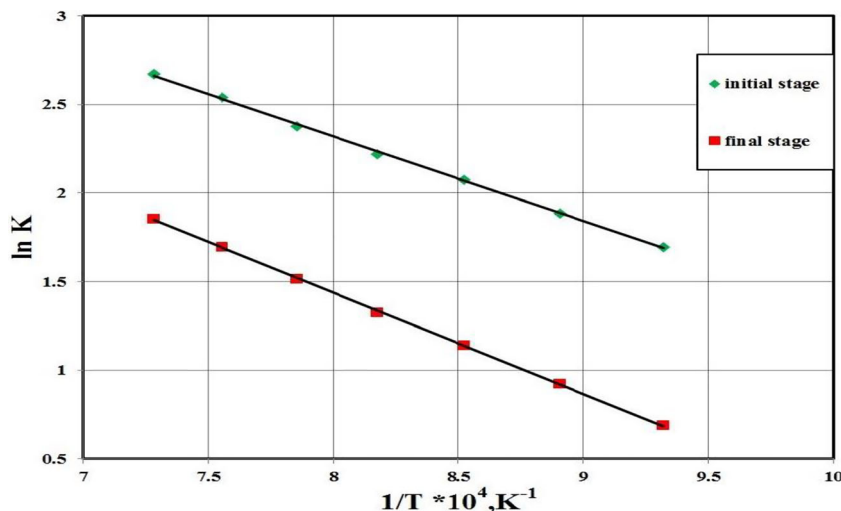
formulations were tested against experimental results as presented in Figs. 7 and 8. During the initial stages, linear correlations were provided from the application of the mixed control mechanism (Eq. 6) as shown in Fig. 7. During the final stages, linear correlations were obtained when applying an interfacial chemical reaction (Eq. 5) as illustrated in Fig. 8. These are consistent with the mechanisms suggested by the activation energy values.

The morphological structures of the reduced samples at 1000 °C during the initial and final stages are shown in Fig. 9a, b, c, d, respectively. Figure 9 a shows the formation of a relatively porous structure which facilitates the access of gas diffusion. Figure 9b shows the formation of the outer/middle interface (red line) of the compact, which is comprised of iron-wustite phase diffusion in the wustite matrix. This indicates that the reducing gas is easily diffused through the outer shell and consequently, iron is nucleated and grows up on the surface of the wustite particles allowing the development of the iron-wustite intergrowth layer. Resistance to gas diffusion decreases near the surface of wustite grains and the chemical

reaction resistance has a major effect as a controlling mechanism. Therefore, mixed mechanism combines gas diffusion and interfacial chemical reaction controlling the reaction. Figure 9c illustrates that the grains of metallic iron are coalescing to each other with small separate macropores. As the reduction proceeds, large macropores are observed due to the coalescing of metallic iron grains as shown Fig. 9d. Accordingly, gas diffusion becomes easier through relatively porous structures, so the reaction is controlled by chemical reaction mechanism.

3.2 Non-Isothermal Reduction

3.2.1 Reduction Behavior

Non-isothermal experiments were carried out at temperatures ranging from room temperature up to 1000 °C in H_2 atmosphere using different heating rates (5, 10, 15, and 20 °C/min). The results are shown in Fig. 10. The heating rate has a considerable effect on the reduction process. The degree of

Fig. 7 Application of mathematical equation at the initial stages of reduction (5–15%)
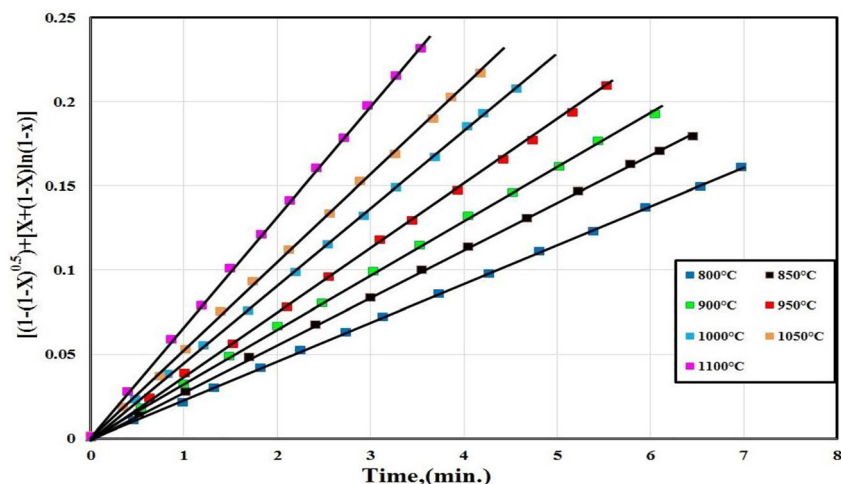
Fig. 8 Application of mathematical equation at the final stages of reduction (85–95%)
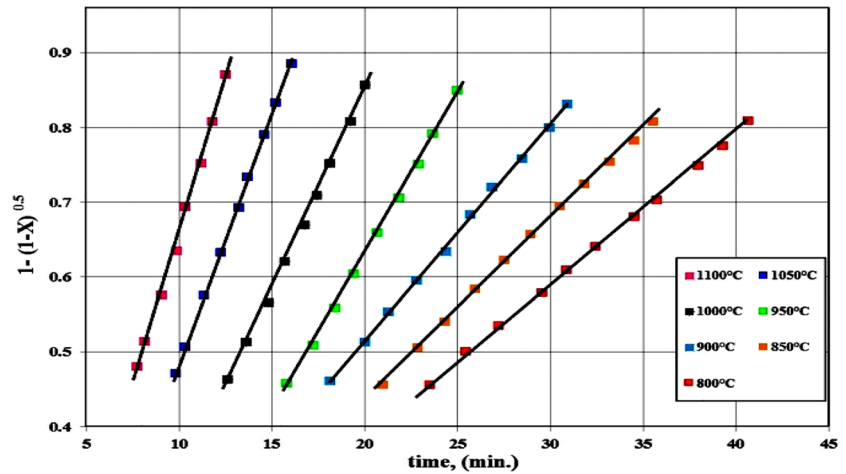
reduction decreases as the heating rate increases. Increasing heating rates leads to shorter time for the sample at any particular temperature. At the same heating rate, the degree of reduction is higher in H_2 than in CO atmosphere [26].

For any given reduction curve presented in Fig. 10, the reduction process can be categorized into three steps:

i. Incubation step, from the beginning up to $\approx$ 400 °C, during which no reduction reaction occurs.
ii. Induction step, from temperature > 400 up to 800 °C, where the reduction rate greatly increases with the rise in temperature and depending on the applied heating rate.
iii. Deceleration step, over 800 °C, at which the reduction rate decreases until the end of experiment.

3.2.2 Kinetics and Mechanism

There are many methods available for evaluating non-isothermal kinetic parameters [33, 34]. This study employs two mathematical analysis methods to determine the kinetic parameters: a model-free isoconversional analysis and model fitting [35, 36].

The overall reaction rate can be generally described by [34]

$$\frac{d\alpha}{dt} = A\exp\left(\frac{-Ea}{Rt}\right)f(\alpha) \qquad (7)$$

Under non-isothermal condition, when the sample is heated at a constant heating rate, the explicit temporal in Eq. 7 is eliminated through the trivial transformation

Fig. 9 RLM photomicrograph ($\times$ 500) of Fe_2O_3 reduced by H_2 at 1000 °C. **a, b** 15% reduction extent at the initial stage. **c, d** 85% reduction extent at the final stage
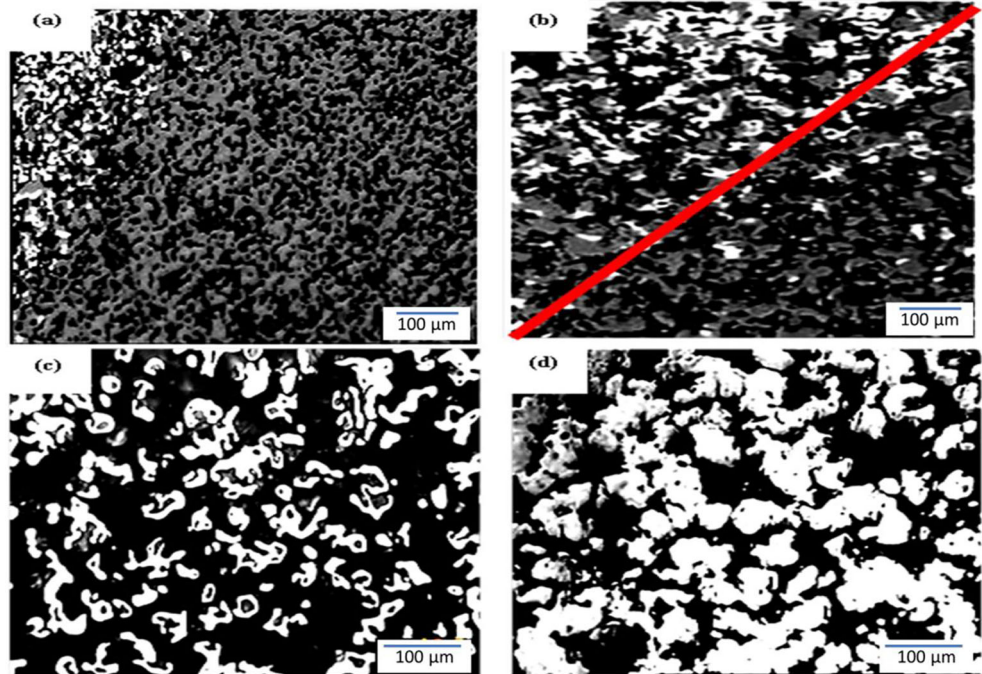
Fig. 10 Effect of heating rates on reduction extent of H$_2$ reaction

was used to determine the kinetic parameters. Coats and Redfern (CR) have provided one of the most popular model-fitting methods [39].
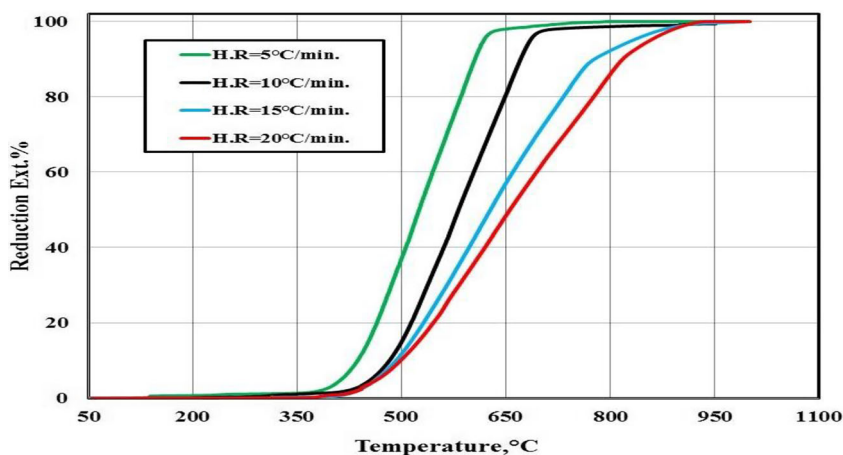
$$\frac{d\alpha}{dT} = \frac{d\alpha}{dt} * \frac{dt}{dT} = \frac{A}{\beta}\exp\left(\frac{-Ea}{RT}\right)f(\alpha) \qquad (8)$$

where β is the heating rate. Upon integration, Eq. (8) gives

$$g(a) = \int_0^a \frac{d(a)}{f(a)} = \frac{A}{\beta}\int_0^T \exp\left(\frac{-Ea}{RT}\right)dT \qquad (9)$$

Model-free isoconversional methods estimate the kinetic parameters without modelistic assumptions [35–37]. The basic assumption of this method is that the reaction rate at a given conversion degree is only a function of temperature [38]. A typical example of this kind of approach is the Kissinger-Akahira-Sunose (KAS Eq. 10) method, which has been widely used to analyze the reaction of kinetic parameters as a function of the conversion degree.

$$\ln\frac{\beta}{T^2} = \ln\left(\frac{AEa}{g(\alpha)R}\right) - \frac{Ea}{RT} \qquad (10)$$

Figure 11 shows the KAS plots of ln β/T^2 against $1/T$ for different conversion degree values. The apparent activation energy values listed in Table 4 were computed using the slopes of the lines drawn. With the increase in reduction during the process, the Ea value becomes smaller and smaller from 92.57 to 20.19.

In order to predict the most probable reduction mechanism, model-fitting methods were employed. The model offering the best statistical fit was chosen as the reaction model that

$$\ln\frac{g(a)}{T^2} = \ln\left(\frac{AR}{\beta Ea}\left[1-\left(\frac{2RT_{\exp}}{Ea}\right)\right]\right) - \frac{Ea}{RT} \qquad (11)$$

where T is the mean experimental temperature and $g(a)$ is a function that mathematically describes the reaction kinetics.

Several models tabulated elsewhere [40] for the integral form $g(\alpha)$ were tested according to CR method. The plot of ln $[g(\alpha)/T^2]$ versus $1/T$ will be linear with a high correlation coefficient. Figure 12 reveals that the Avrami-Erofeev model provides a linear trend with a correlation coefficient (R) higher than 0.99, indicating that the reduction is controlled by the Avrami-Erofeev model.

The calculated activation energy values (Ea) at different conversion degrees (α) are presented in Fig. 13. Higher activation energy values were obtained at earlier stages and decrease as the reduction extents increased. The reduction starts at a lower temperature and requires high energy (Ea) to proceed. The decreasing in Ea values can be attributed to the effect of temperature, which has a considerable effect on the reduction process.

The morphological changes in the completely reduced samples at 20 °C/min and 5 °C/min analyzed using an SEM microscope are shown in Fig. 14a and b, respectively. Figure 14a illustrates that the microstructure of iron ore includes significant porosity and the formation of metallic iron whiskers. Furthermore, the formation of dense structures of

Table 4 Apparent activation energy values computed at overall reduction reaction

Conversion degree (α)	0.1	0.2	0.3	0.4	0.5	0.6	0.7	0.8	0.9	1
Ea value	92.57	79.34	66.71	56.89	45.21	38.97	33.96	30.03	25.61	20.19

Fig. 11 Kissinger plot at different reduction extents of Fe_2O_3 reduced by H_2
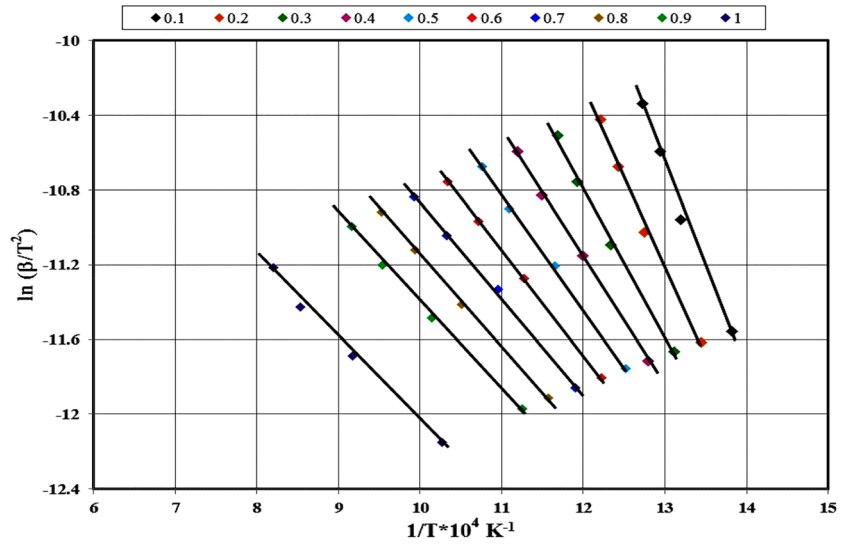
Fig. 12 Coats-Redfern plot of reduction of iron ore compacts with H_2 gas
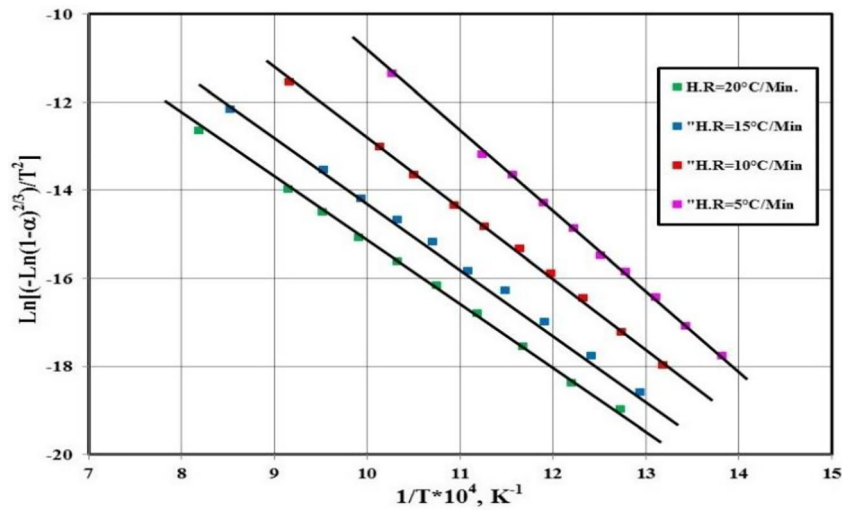
Fig. 13 Calculation Ea against conversion degree of iron ore compact reduced by H_2
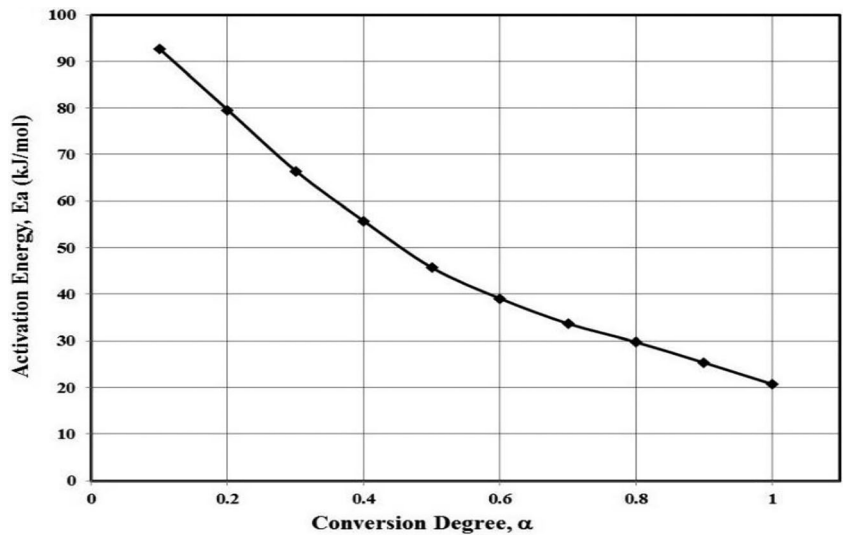
Fig. 14 SEM images of iron oxide fines non-isothermally reduced with H_2 up to 1000 °C. **a** HR = 20 °C/min. **b** HR = 5 °C/min
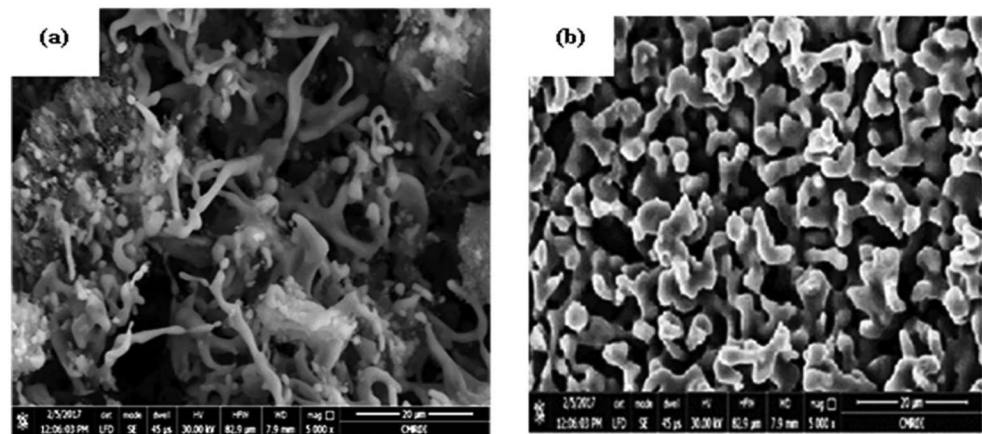
metallic iron grain results from the connections between the metallic iron grains as shown in Fig. 14b.

The microstructure of fully reduced samples at different heating rates (20, 15, 10, and 5 °C/min) examined by a reflected light microscope is presented in Fig. 15a–d. It can be observed that the heating rate has an obvious effect on the structure of the iron grains. Figure 15a (20 °C/min) shows a structure that includes bright white grains of metallic iron scattering all over the matrix. Figure 15b (15 °C/min) illustrates that the grains of metallic iron connected together forming a relatively dense matrix with small separate macropores. By decreasing the heating rate as shown in Fig. 15c (10 °C/min), the matrix includes large grains of metallic

iron which contain micropores. As shown in Fig. 15d (5 °C/min), denser structure can be observed attributable to sintering and the connection of metallic iron grains. These above results indicate that the microstructure of samples becomes denser as the heating rate decreases. This is most likely attributable to the relatively longer reaction time, which allows more time for growth of the metallic iron grains.

Figure 16 shows the XRD patterns of non-isothermal reduction products at different heating rates and at 1000 °C. The intensity of the metallic iron peaks increases as heating rates decrease, because of the longer retention time of the sample, and consequently enhances the recrystallization of the iron phase, which is evident from Fig. 15.

Fig. 15 RLM photomicrograph of iron ore fines non-isothermally reduced at 1000 °C (× 500). **a** 20 °C/min. **b** 15 °C/min. **c** 10 °C/min. **d** 5 °C/min
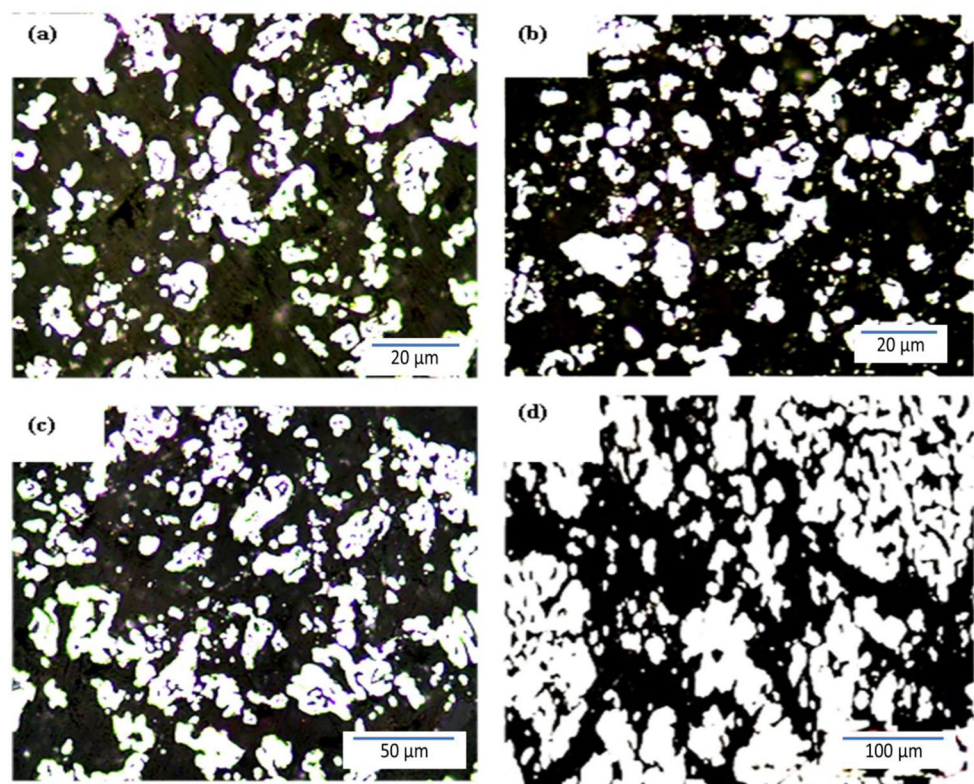
Fig. 16 XRD patterns of the samples reduced by H_2 at four heating rates
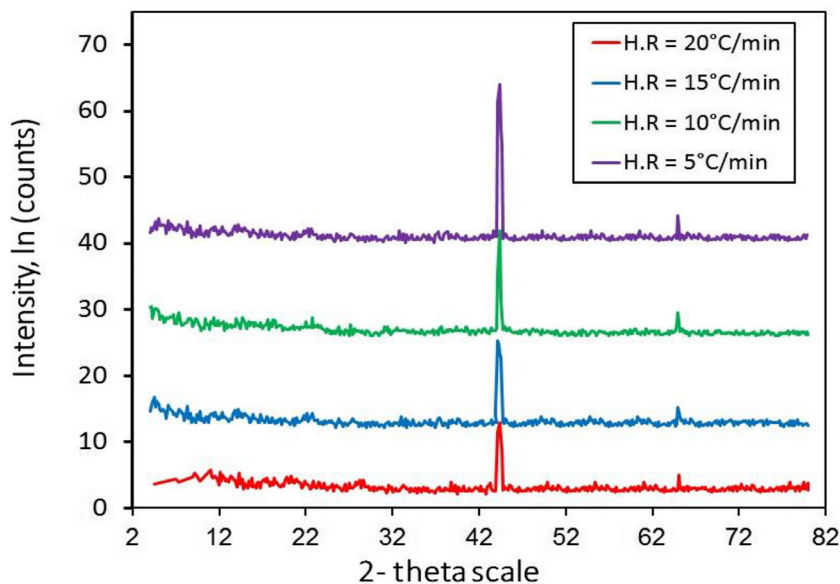
4 Conclusion

Understanding the kinetic analysis of non-isothermal conditions is helpful in the DR process and in hydrogen metallurgy. The latter has become important topic in the global steel industry and in academic fields in recent years. It provides promising solution that could be very effective in decreasing the CO_2 emissions and also metallurgical coke utilization in iron and steel industry by optimization of hydrogen-rich materials such as natural gas in the ironmaking processes. Such solutions require intensive investigations in order to understand and precisely evaluate their influence on iron and steel industry and CO_2 mitigation. This study investigated isothermal and non-isothermal reductions of iron ore fines in a pure H_2 atmosphere. In the experiments, total weight loss was continuously recorded using TG and the kinetic mechanisms were studied. The experimental results and kinetic analyses suggest the following conclusions:

1. Temperature plays a significant role in the isothermal reduction process. The reduction rate during the initial stages is higher than the reduction rate during the final stages.
2. The rate-controlling mechanism of the reduction process was predicted using an activation energy calculation, through applying gas-solid mathematical models, and microstructure examination. During the initial stages, the reduction reaction was controlled by a mixed mechanism of interfacial chemical reaction and gas diffusion. During the final stages, the interfacial chemical reaction was the rate-determining step.
3. The heating rate has a significant effect on the reduction rate and reduction conversion for non-isothermal reductions. With identical heating rates, the degree of reduction was higher in H_2 than in CO atmosphere.
4. The kinetic mechanisms of the reductions could be predicted by applying model-free and model-fitting methods. The wide range of activation energy values (92.57 to 20.19) in the model-free approach was mainly a result of temperature differences. When applying the Coats-Redfern method, the reduction reaction was controlled by the Avrami-Erofeev model.

Compliance with Ethical Standards

Conflict of Interest The authors declare that they have no conflict of interest.

References

1. Pardo N, Moya JA (2013) Prospective scenarios on energy efficiency and CO_2 emissions in the European Iron & Steel industry. Energy 54:113–128

2. Mousa E, Wang C, Riesbeck J, Larsson M (2016) Biomass application in iron and steel industry: an overview of challenges and opportunities. Renew Sustain Energy 65:1247–1266

3. World Steel Association (2018) Steel Statistical Yearbook 2018, vol 20. World Steel Association, Brussels

4. Ahmed H (2018) New trends in the application of carbon-bearing materials in blast furnace ironmaking. Minerals 8(12):561

5. International Energy Agency (2010) Energy technology perspectives: scenarios and strategies to 2050, Paris, France.

6. Wang X, Lin B (2016) How to reduce CO_2 emissions in China's iron and steel industry. Renew Sust Energ Rev 57:1496–1505

7. Wright JK, Taylor I, Philp DK (1991) A review of progress of the development of new ironmaking technologies. Miner Eng 47:983–1001

8. Olsson, O (2018) Low-emission steel production: decarbonising heavy industry. Available online: https://www.sei.org/perspectives/low-emission-steel-production-hybrit (accessed on 11 April 2018).

9. Quailan H (2019) Hydrogen as a clean alternative in the iron and steel industry. http://www.fchea.org/in-transition/2019/11/25/hydrogen-in-the-iron-and-steelindustry.

10. Pasquale C (2019) Clean ironmaking and steelmaking processes efficient technologies for greenhouse emissions abatement.

11. Abdelrahim A, Iljana M, Omran M, Vuolio T, Bartusch H, Fabritius T (2020) Influence of H_2-H_2O content on the reduction of acid iron ore pellets in a CO-CO_2-N_2 reducing atmosphere. ISIJ Int. https://doi.org/10.2355/isijinternational.ISIJINT-2019

12. Spreitzer D, Schenk J (2019) Reduction of iron oxides with hydrogen-a review. Steel Res Int 90:1900108. https://doi.org/10.1002/srin.201900108

13. El-Geassy AA, Shehat KA, Ezz SY (1977) Mechanism of iron oxide reduction with hydrogen/carbon monoxide mixtures. Trans ISIJ 17:629

14. El-Geassy AA (1999) Influence of doping with CaO and/or MgO on stepwise reduction of pure hematite compacts. Ironmak Steelmak 26(1):41

15. El-Geassy AA, Nasr MI, Hessein MM (1996) Effect of reducing gas on the volume change during reduction of iron oxide compacts. ISIJ Int 36:640

16. Nasr MI, Omar AA, Hessein MM, El-Geassy AA (1996) Carbon monoxide reduction and accompanying swelling of iron oxide compacts. ISIJ Int 36(2):164

17. Strangway PK (1964) Kinetics of reduction of iron oxide by reformed natural gas. M.Sc. Thesis, Metallurgy and Materials Science, Toronto University.

18. Spreitzer D, Schenk J (2019) Iron ore reduction by hydrogen using a laboratory scale fluidized bed reactor: kinetic investigation-experimental setup and method for determination. Metall Mater Trans A 50B:2471

19. Lin HY, Chen YW, Li C (2003) The mechanism of reduction of iron oxide by hydrogen. Thermochim Acta 400:6

20. Piotrowski K, Mondal K, Lorethova H, Stonawski L, Szymanski T, Wiltowski T (2005) Effect of gas composition on the kinetics of iron oxide reduction in a hydrogen production process. Int J Hydrog Energy 30(15):1543–1554

21. Bonalde A, Henriquez A, Manrique M (2005) Kinetic analysis of the iron oxide reduction using hydrogen/carbon monoxide mixtures as reducing agent. ISIJ Int 45(9):1255–1260

22. Skorianz M (2012) Ph.D. Thesis, Montan University Leoben.

23. GeonYong L, Song J, JaiSung L (2016) Reaction kinetics and phase transformation during hydrogen reduction of spherical Fe_2O_3 nanopowder agglomerates. Powder Technol 302:215–221

24. Dang J, Guohua Z, Xiaojun H, Kuochih C (2013) Non-isothermal reduction kinetics of titanomagnetite by hydrogen. Int J Miner Metall Mater 20:1134

25. Tiernan MJ, Barnes PA, Parkes GM (2001) Reduction of iron oxide catalysts: the investigation of kinetic parameters using rate perturbation and linear heating thermoanalytical techniques. J Phys Chem 105B:220–228

26. El-Geassy AA, Nasr MI, El-Raghy SM, Hammam AA (2019) Comparative studies on isothermal and non-isothermal reduction of hematite in carbon monoxide atmosphere. Ironmak Steelmak. https://doi.org/10.1080/03019233.2019.1646564

27. EI-Geassy AA (1986) Gaseous reduction of Fe_2O_3 compacts at 600 to 1050 °C. Mater Sci 21(11):3889–3900

28. Szekely J, Evans JW, Sohn HV (1976) Gas-solid reaction. Academic press, New York

29. Sohn H, Szekely J (1972) A structural model for gas-solid reactions with a moving boundary III: a general dimensionless representation of the irreversible reaction between a porous solid and a reactant gas. Chem Eng Sci 27(4):763–778

30. Seth BL, Ross HU (1965) Mechanism of iron oxide reduction. Trans Metall Soc AIME 233(1):180–185

31. McKewan WM (1960) Kinetics of iron oxide reduction. Trans Am Instit Min Metall Eng 218(1):2–6

32. El-Geassy AA (1996) Reduction of CaO and/or MgO-doped Fe_2O_3 compacts with carbon monoxide at 1173-1473 K. ISIJ Int 36(11):1344

33. Šimon P (2004) Isoconversional methods. J Therm Anal Calorim 76(1):123–132

34. Sbirrazzuoli N, Vincent L, Mija A, Guigo N (2009) Integral, differential and advanced isoconversional methods: complex mechanisms and isothermal predicted conversion–time curves. Chemom Intell Lab Syst 96(2):219–226

35. Khawam A, Flanagan DR (2005) Role of isoconversional methods in varying activation energies of solid-state kinetics: I. Isothermal kinetic studies. Thermochim Acta 429(1):93–102

36. Khawam A, Flanagan DR (2005) Role of isoconversional methods in varying activation energies of solid-state kinetics: II. Nonisothermal kinetic studies. Thermochim Acta 436(1):101–112

37. Vyazovkin S (2000) Computational aspects of kinetic analysis: part C. The ICTAC kinetics project-the light at the end of the tunnel. Thermochim Acta 355(1):155–163

38. Burnham AK (2000) Computational aspects of kinetic analysis, part D: the ICTAC kinetics project-multi-thermal–history model-fitting methods and their relation to isoconversional methods. Thermochim Acta 355(1):165–170

39. Coats A, Redfern J (1964) Kinetic parameters from thermogravimetric data. Nature 201:68

40. Sun Y, Han Y, Wei X, Gao P (2016) Non-isothermal reduction kinetics of oolitic iron ore in ore/coal mixture. J Therm Anal Calorim 123(1):703–715